Local control of magnetic interface effects in chiral Ir|Co|Pt multilayers using Ga⁺ ion irradiation

Mark C. H. de Jong [ORCID],[*] Mariëlle J. Meijer, Juriaan Lucassen [ORCID], Jos van Liempt [ORCID], Henk J. M. Swagten,
Bert Koopmans, and Reinoud Lavrijsen [ORCID]

Department of Applied Physics, Eindhoven University of Technology, P.O. Box 513, 5600 MB Eindhoven, the Netherlands

In this work we investigate local tuning of the iDMI and perpendicular magnetic anisotropy (PMA) using focused Ga⁺ ion beam irradiation, in an Ir|Co|Pt multilayer system. We show that the magnitude of the interface contribution to both effects can be significantly reduced by the irradiation with Ga⁺ ions. This leads to a reduction by a factor of 2 of the domain wall energy density, while still preserving the Néel character of the domain walls. Hence, we postulate that Ga⁺ ion irradiation is an effective way to locally reduce the energy barrier for skyrmion nucleation, providing a novel pathway for targeted skyrmion nucleation in racetrack type devices.

I. INTRODUCTION

Chiral magnetic textures such as skyrmions have shown great promise as data carriers in future spintronic memory devices [1–5]. Their spin texture consists of a circular domain, surrounded by a domain wall with a uniform chirality. They can be very small, with diameters down to a few nanometers [4,6], can be moved efficiently using electrical current pulses [7], and are very stable [6]. This stability is a direct result of the uniform chirality of the domain wall [8], which ensures that the topology of the skyrmion magnetization texture is different than the ferromagnetic background, which contributes to the energy barrier that prevents their annihilation [9]. These properties make chiral textures and specifically skyrmions interesting objects for future logic and data storage devices.

Chiral textures are stabilized by an asymmetric exchange interaction called the Dzyaloshinskii-Moriya interaction (DMI), which originates from the spin-orbit coupling in combination with inversion symmetry breaking [10,11]. This interaction prefers a perpendicular alignment of neighboring spins, with a well-defined chirality and hence stabilizes homochiral spin structures such as skyrmions. These have been observed in many physical systems with a DMI [4,12,13], but this article will focus on magnetic multilayers, in which room temperature stable Néel skyrmions were first observed [7,14,15]. In these systems the DMI originates from the interfaces between magnetic and heavy-metal layers. However, such an interface DMI (iDMI) is often not strong enough to stabilize skyrmions in single magnetic layers at room temperature. Therefore, many magnetic layers are stacked on top of each other to increase the magnetic volume, increasing the effect of the magnetic dipole field and thereby the thermal stability [14]. Many different combinations of materials have been shown to support room temperature skyrmions, e.g., Refs. [4,6,7,14–24], suggesting that skyrmions can be stabilized for a wide range of magnetic parameters. These

parameters can then be readily tuned by varying the layer thickness or through material choices, allowing for the optimization of the skyrmion energy cost [16].

However, these attributes can usually only be changed for the entire layer or device. The ability to locally control these magnetic parameters could greatly enhance the functionality of skyrmion based devices [25–28], or devices that use other types of chiral textures. Enabling the creation of regions with high and low energy that could then be used to pin, guide [25–28], or nucleate [17,29,30] such textures at desired locations in the device. It has already been well established that Ga⁺ and other types of ion irradiation can be used to locally tune the magnetic parameters of single magnetic layers in areas as small as 40 nm [31–34], but its effect on magnetic multilayers is not yet understood. Very recently, a study investigating the effect of low energy, broad beam He⁺ ion irradiation on [Pt|Co|Ta]×10 multilayers reported that the magnetic parameters can indeed be controlled, similar to a single magnetic layer [35]. However, compared to He⁺ ions, the penetration depth of Ga⁺ ions is much lower [35,36] and therefore it is not immediately obvious that Ga⁺ ions can also significantly affect the effective magnetic properties of the multilayer stack.

In this article we present the results of a systematic study on the effects of local Ga⁺ion irradiation on the magnetic parameters in an Ir|Co|Pt multilayer, in particular the effective anisotropy K_{eff} and the iDMI D. We will first present Hall effect measurements of the change in the effective anisotropy as a result of the Ga⁺ irradiation [37,38]. We find that the effective anisotropy of the stack can be readily decreased through the irradiation with Ga⁺ ions, in line with work on single magnetic layers. Next, we combine these measurements with magnetic force microscopy (MFM) measurements of the stripe domain state [39,40] to determine how the effective iDMI of the multilayer is affected by the Ga⁺ ion irradiation and show that the iDMI also decreases in magnitude. When we only consider the interface contribution to each effect, we find that the relative decrease is the same for the anisotropy and iDMI which shows that both effects depend similarly
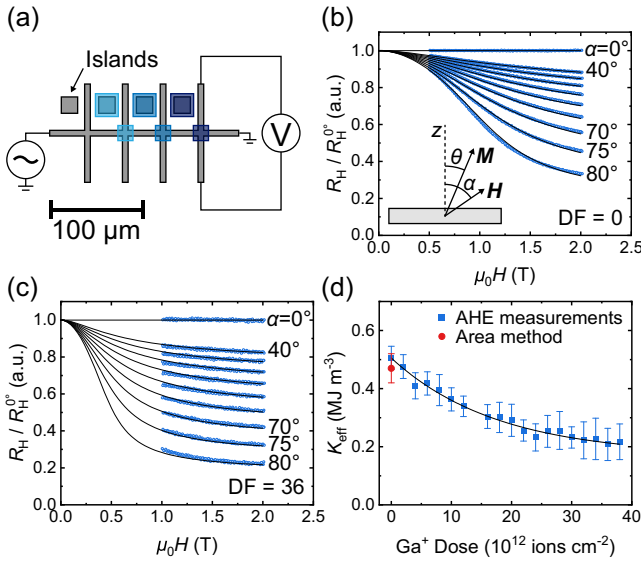
*m.c.h.d.jong@tue.nl

FIG. 1. (a) Schematic overview of the Hall bar devices. Each Hall cross has been irradiated with a different Ga^+ dose, indicated by different shades of blue. The islands in between the Hall bars are also irradiated, with the same dose as the Hall cross to their bottom right. (b) The Hall resistance measured during field sweeps from $\mu_0 H = 2$ T to $\mu_0 H = 0$ T (blue circles), for different angles α, fitted using the Stoner-Wohlfarth model measured on a nonirradiated sample (black lines). Data points below $\mu_0 H = 0.5$ T are not plotted to improve the clarity, but the agreement with the fit is equally good. The inset shows the definition of the angles α and θ. DF indicates the dose factor, i.e., the dose is $d = DF \times 10^{12}$ ions cm^{-2}. (c) The same measurement as in (b) performed on a Hall cross that has been irradiated with a dose of $d = 36 \times 10^{12}$ ions cm^{-2}. The measurement is performed for $\mu_0 H = 2$ T to $\mu_0 H = 1$ T. (d) Plot of K_{eff}, determined using the AHE measurements shown in (b) and (c), plotted as a function of Ga^+ dose.

on the interface quality and the degree of intermixing. This tuning of the magnetic parameters leads to a reduction in the domain wall energy density up to a factor of 2, while still preserving the Néel character of the domain walls. Hence, we postulate that ion irradiation is also an effective way to reduce and control the energy cost of different chiral structures in magnetic multilayers, such as skyrmions.

II. METHODS

The complete material stack that is investigated in this article is $||Ta(4)|Pt(2)|[Ir(1)|Co(0.8)|Pt(1)]_{\times 6}|Pt(2)$ on top of a $Si|SiO_2(100)||$ substrate. The numbers in the brackets indicate the layer thickness in nm. All layers are grown using DC magnetron sputtering at a base pressure better than $P = 1 \times 10^{-8}$ mbar in an argon atmosphere with a partial pressure of $P = 2 \times 10^{-3}$ mbar. The material stack is patterned into the Hall bar structures shown schematically in Fig. 1(a) using standard electron beam lithography and lift-off. Following the patterning several regions of the devices are irradiated with Ga^+ ions using a FEI Nova Nanolab 600 Dualbeam operated at a beam current of 1.5 pA and an acceleration voltage of 30 keV. Different regions on the devices are irradiated with different doses by varying the dwell time of the Ga^+ beam,

indicated by the shaded blue regions in Fig. 1(a). In total seven different devices were used in this study, grown during two separate deposition runs.

To measure the local change in the anisotropy due to the ion irradiation we will determine the anisotropy from electrical Hall measurements [37]. To this end, the Hall cross corresponding to this dose is electrically connected as shown in Fig. 1(a). The first harmonic Hall resistance is measured by sending an AC current with a RMS current density of $j = 1 \times 10^6$ A/m^2 and frequency $f = 901$ Hz through the current line, the resulting Hall voltage is then measured using a lock-in amplifier.

The strength of the iDMI will be determined from MFM measurements of the stripe domain state and a recently developed model of the equilibrium stripe domain width [39]. We follow the experimental procedure outlined in Ref. [40] to determine the strength of the DMI using this model. It takes as input the geometry of the multilayer stack and the magnetic parameters (A, M_s, K_{eff}, and D) and gives a value for the equilibrium domain width W_{eq}. We then calculate the expected domain size W_{eq} for a range of DMI values between 0 and 2.5 mJ m^{-2} (steps of $\Delta D = 0.05$ mJ m^{-2}) and interpolate to find the curve $W_{eq}(D)$. Using this curve we can determine which value of D correspond to the stripe domain width observed in our magnetic multilayer [40–42].

The stripe domain width is determined from the 2D fast Fourier transform (FFT) of a 10×10 μm^2 MFM scan of the stripe domain state. These scans are taken on the irradiated 20 μm wide squares in between the Hall bars [labeled Islands in Fig. 1(a)] with MFM, on a Brüker dimension edge with custom coated low-moment tips. The irradiation of these islands was done at the same time as the Hall cross with the corresponding dose. To bring the magnetization of the multilayers into the stripe domain state, the devices shown in Fig. 1(a) are demagnetized in an oscillating magnetic field, with the field oriented approximately 85° away from the sample normal [41]. The field strength starts at 5 T and is gradually reduced by 0.5% after each oscillation, until a threshold value of 10 mT is reached. After this procedure, the magnetization inside the islands shown in Fig. 1(a) exhibits a stripe domain state for all the Ga^+ doses studied.

The saturation magnetization M_s and the effective anisotropy K_{eff} of an unpatterned sample are measured using a SQUID-VSM and the area method (where K_{eff} is determined from the area in between the easy and hard axis loops [43]). We find $M_s = 1.01 \pm 0.04$ MA m^{-2} and $K_{eff} = 0.47 \pm 0.05$ MJ m^{-3}, respectively. These values are comparable to our previous work [44]. (See Appendix A for the SQUID-VSM measurement).

III. RESULTS AND DISCUSSION

A. Anisotropy as a function of ion dose

We will first present the electrical Hall measurements that were used to determine the dependence of the effective anisotropy K_{eff} on the Ga^+ ion dose. The measured Hall voltage is proportional to M_z, the average out-of-plane component of the magnetization **M** in the region where the current line and Hall arms cross, through the anomalous Hall effect [45]. During the measurement a magnetic field is applied at

an angle α to the z direction [inset in Fig. 1(b)]. The effect of this field on the magnetization is to pull it away from its equilibrium out-of-plane orientation towards the in-plane direction, by an angle θ. The rotation of **M** is resisted by the effective anisotropy such that a stronger K_{eff} results in a smaller θ. This behavior is described by the Stoner-Wohlfarth model [43],

$$E_{\text{tot}} = K_{\text{eff}} \sin^2(\theta) - \mu_0 H M_s \cos(\alpha - \theta), \quad (1)$$

minimizing E_{tot} with respect to θ gives an implicit function for θ which we will use to determine the effective anisotropy.

In Fig. 1(b) we have plotted the normalized first harmonic Hall resistance R_{H} measured using a nonirradiated Hall cross. Shown are several field sweeps starting from $\mu_0 H = 2.0$ T to $\mu_0 H = 0$ T, for different angles α between the field and the sample normal. All measurements are normalized to the Hall resistance measured for $\alpha = 0°$. As expected, a larger field and angle result in a smaller R_{H}, since the magnetization is pulled further in-plane. The black lines in Fig. 1(b) are fits to the data using the Stoner-Wohlfarth model, where K_{eff} is the only fitting parameter. All field sweeps are fitted at the same time, resulting in one value for K_{eff} that describes the measurements for all α. We find a good agreement between the data and the fit. For the nonirradiated Hall cross the fit gives $K_{\text{eff}} = 0.51 \pm 0.04$ MJ m^{-3}, which is in good agreement with the value found using the area method ($K_{\text{eff}} = 0.47 \pm 0.05$ MJ m^{-3}). The uncertainty in the value determined using the Hall measurements comes from the uncertainty in the value of M_s, determined independently from the SQUID-VSM measurement.

Next, we present a similar measurement on a Hall cross irradiated with a Ga$^+$ dose of $d = 36 \times 10^{12}$ ions cm^{-2} in Fig. 1(c). At this dose the sample is no longer in a single domain state at zero field and hence the Stoner-Wohlfarth model no longer describes the behavior of the magnetization in the low field region. Therefore, we only fit the data for the part of the field sweep from $\mu_0 H = 2.0$ T to $\mu_0 H = 1.0$ T, where the field is strong enough to ensure a uniform magnetization, as assumed by the Stoner-Wohlfarth model. In this field range we again find good agreement between the data and the fit and determine a value for the effective anisotropy of $K_{\text{eff}} = 0.21 \pm 0.06$ MJ m^{-3}. Compared to the nonirradiated sample the anisotropy is reduced by more than a factor of 2. Here we have assumed that the saturation magnetization is not affected by the ion irradiation, as expected for Pt|Co|Pt based thin films [46]. Nevertheless, we show in Appendix B that a small change in the magnetization as a function of dose will not qualitatively affect the results presented.

This procedure to measure K_{eff} is performed for Ga$^+$ doses up to $d = 38 \times 10^{12}$ ions cm^{-2} and in Fig. 1(d) we plot the measured effective anisotropy as a function of Ga$^+$ dose. For all measurements, the AHE data was only fitted in the field range between $\mu_0 H = 2.0$ T to $\mu_0 H = 1.0$ T, to ensure a single domain response as required by the Stoner-Wohlfarth model. At low Ga$^+$ doses, between 0 and $d = 16 \times 10^{12}$ ions cm^{-2}, we observe a strong decrease in the measured anisotropy which gradually slows down for higher doses. The black line is a fit to the data and shows that the effective anisotropy decreases exponentially to a constant nonzero

value as a function of the ion dose. This behavior is consistent with previous work on Pt|Co|Pt single magnetic layers [36,38], for low ion doses.

The change in the anisotropy in such systems is, in part, attributed to an increase in the amount of directional intermixing, as the collision cascade of the Ga$^+$ ions is top down, of the heavy metal and Co atoms at the interfaces [36,46]. This effectively makes the transition between the heavy metal layer and the Co layer smoother, which results in a more symmetric environment for the Co atoms at the interface. We speculate that the same mechanism affects the strength of the iDMI and, in particular, causes a decrease in the iDMI strength as a function of Ga$^+$ dose due the reduction of the inversion symmetry breaking at the two interfaces. *Ab initio* simulations indeed predict a (small) decrease in the iDMI strength upon intermixing of a Pt|Co interface [47,48]. Additionally, Ga$^+$ ion implantation at the interfaces might influence the strength of the anisotropy and iDMI as well [36,48]. However, we believe that the contribution from this effect is small in our samples as the number of Ga$^+$ ions is much lower than the number of Pt, Co, and Ir atoms. In the remainder of this article we will investigate the dependence of the iDMI on Ga$^+$ ion irradiation experimentally.

B. Calculating the iDMI strength

Now that the dependence of K_{eff} on the Ga$^+$ dose is known, we will focus on determining the change in the strength of the iDMI using the model of Lemesh *et al.* [39]. To this end we imaged the stripe domain state in the irradiated Ir|Co|Pt multilayers using MFM, as described in the Methods section. In Figs. 2(a)–2(d) we show the MFM measurements of the stripe domain state for four different Ga$^+$ doses, $d = 0$ ions cm^{-2}, $d = 10 \times 10^{12}$ ions cm^{-2}, $d = 20 \times 10^{12}$ ions cm^{-2}, and $d = 30 \times 10^{12}$ ions cm^{-2} for (a)–(d), respectively. The scale bar for all four images is identical and hence it is immediately clear that Ga$^+$ irradiation has a strong effect on the domain size. For increasing dose we observe a strong decrease of the domain width. To quantify this change we measure the domain width in each MFM scan using the 2D FFT (described in detail in Ref. [49]). We confirmed that the equilibrium domain size in the nonirradiated islands is the same as the measured domain size in an unpatterned sample (not shown).

The measured domain size W_{MFM} is plotted against the Ga$^+$ dose in Fig. 2(e). Qualitatively, the observed trend in the domain size is similar to the observed trend for the effective anisotropy. Until a Ga$^+$ dose of approximately $d = 12 \times 10^{12}$ ions cm^{-2} the domain width decreases rapidly as a function of dose. This decrease slows down for higher doses and eventually saturates around $W_{\text{MFM}} = 140 \pm 2$ nm. The decrease in the domain size can be understood by considering the domain wall energy density [50],

$$\sigma_{\text{DW}} = 4\sqrt{A K_{\text{eff}}} - \pi |D|. \quad (2)$$

As the effective anisotropy decreases, the energy cost of a domain wall also decreases, resulting in an increase in the number of domain walls and narrower domains. Comparing Figs. 1(d) and 2(e) we see that the dependence of K_{eff} and W_{MFM} on the Ga$^+$ dose differ for high doses (i.e., $d > 20 \times 10^{12}$ ions cm^{-2}). The domain width remains constant
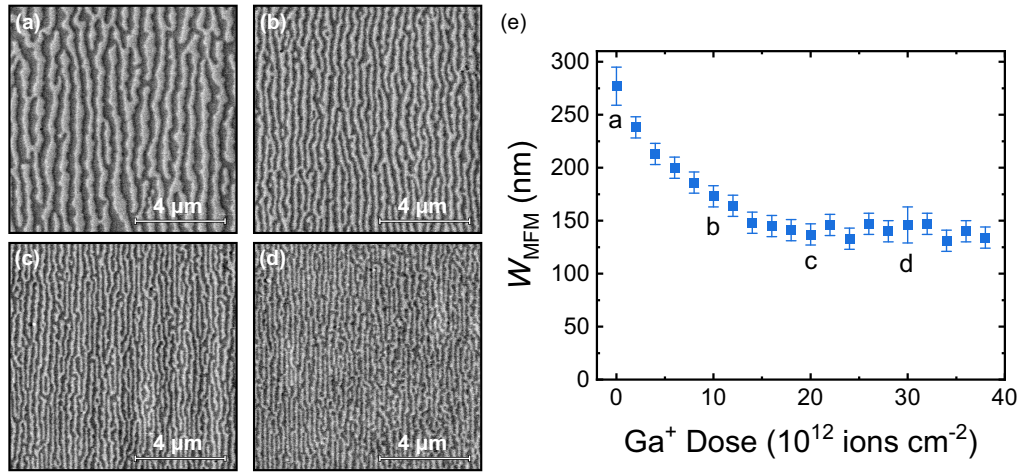
FIG. 2. (a)–(d) MFM measurements of the stripe domain state in the magnetic multilayer before and after irradiation with Ga^+ ions. The Ga^+ dose for each image is: (a) $d = 0 \times 10^{12}$ ions cm^{-2}, (b) $d = 10 \times 10^{12}$ ions cm^{-2}, (c) $d = 20 \times 10^{12}$ ions cm^{-2}, and (d) $d = 30 \times 10^{12}$ ions cm^{-2}. (e) Plot of the average domain width, determined from MFM scans, as a function of the Ga^+ ion dose.

while the anisotropy continues to decrease, suggesting that the magnitude of the iDMI should also decrease in this regime to keep σ_{DW} constant.

To quantify this change we use the aforementioned model to calculate the value of the iDMI using the measured values for K_{eff} and W_{MFM}, for the saturation magnetization we use $M_s = 1.01 \pm 0.04$ A m^{-2}, as measured for the nonirradiated sample and for the exchange stiffness we use a value of $A = 10$ pJ m^{-1}, in accordance with other work on similar multilayers [14,41]. In Appendix C we show that the value of A does not impact our findings qualitatively, only quantitatively. Uncertainties in the value of D are calculated using the same procedure as in Ref. [40].

The magnitude of the iDMI is plotted as a function of the Ga^+ dose in Fig. 3(a). Without Ga^+ irradiation we measure an iDMI of $|D| = 1.7 \pm 0.2$ mJ m^{-2}, which is consistent with measurements performed by other groups on similar material stacks [41,42]. We observe that the strength of the iDMI gradually decreases over the entire dose range studied here, down to $|D| = 1.3 \pm 0.2$ mJ m^{-2} for the largest Ga^+ dose ($d = 38 \times 10^{12}$ ions cm^{-2}). This is consistent with the hypothesis that the increase in the degree of intermixing is responsible for the observed changes in K_{eff} and D. The red line in Fig. 3(a) corresponds to the minimum iDMI strength D_{Thr} required to ensure the formation of Néel walls over Bloch walls [39]. We find that the measured iDMI values are at least a factor of 2 greater than this threshold, for all doses, indicating that the irradiation will not affect the chirality of the domain walls in the multilayer.[1]

Next, we compare the observed change in the anisotropy and iDMI. To this end we calculate the interface contribution

to each effect, K_s and D_s for the anisotropy and DMI, respectively. The conversion is done using the following relations:

$$K_{eff} = \frac{2K_s}{t_{Co}} - \frac{1}{2}\mu_0 M_s^2, \qquad (3)$$

$$D = \frac{2D_s}{t_{Co}}. \qquad (4)$$

The factor 2 in front of the interface contribution in each equation accounts for the fact that there are two heavy metal interfaces with the Co layer. This means that K_s and D_s are the average interface contributions of the Ir and Pt interfaces, as we have no method to distinguish between the two.

In Fig. 3(b) we plot the interface contribution to the iDMI against the interface contribution to the anisotropy. Increasing the Ga^+ dose results in a decrease of both D_s and K_s as indicated by the arrow. The data are fitted with a straight line (solid black line), which fits the data well in the studied dose range. Thus the relative decrease in D_s and K_s is the same upon irradiation with Ga^+ ions, suggesting that the dependence on the degree of intermixing at the interface is the same for both effects (in the studied dose range). This result is in line with earlier studies, where the interfaces responsible for the iDMI and anisotropy are modified using annealing [54], He^+ ion irradiation on single magnetic layers [33], or through the crystal phase [55]. In all cases, a correlation between the interface contributions to the anisotropy and iDMI was reported.

The effect of the these changes in the anisotropy and iDMI on the domain wall energy is shown in Fig. 3(c). Here we plot the domain wall energy density, calculated using Eq. (2), as a function of the Ga^+ dose. In the studied dose range, we can reduce the domain wall energy density by a factor of 2. Taken together with the fact that the iDMI always remains larger than the threshold value for Néel type domain walls [Fig. 3(a)], we conclude that Ga^+ ion irradiation is an effective way to decrease the energy cost of chiral domain walls. Decreasing the domain wall energy also decreases the energy of chiral textures such as skyrmions, which has been shown to result in

---

[1]This threshold value does not include the effect of hybrid chiralities due to the dipolar interactions [41,51,52], which might affect the chirality of the domain walls. In Appendix E we show using MuMax³ [53] that it is likely that the chirality in the multilayer is still uniform after irradiation, even at the highest dose used, $d = 38 \times 10^{12}$ ions cm^{-2}.
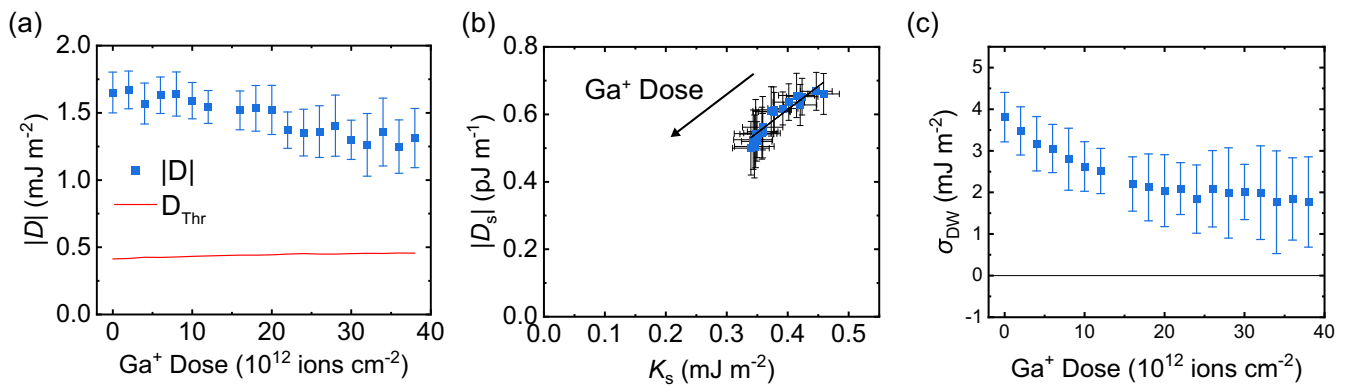
FIG. 3. (a) Plot of the calculated magnitude of the iDMI as a function of the Ga^+ dose (blue). The red line is the threshold iDMI value D_{thr} above which the domain walls are of the Néel type. (b) The interface DMI D_s plotted as a function of the interface anisotropy K_s. In the measured dose range, the relative decrease in D_s and K_s is approximately the same. (c) The domain wall energy density σ_{DW} plotted as a function of the Ga^+ dose.

more efficient field driven nucleation [16]. Hence, we conjecture that Ga^+ ion irradiation can also be used to locally tune the energy and properties of chiral magnetic textures such as skyrmions in multilayer systems.

IV. DISCUSSION AND CONCLUSION

We have shown that magnetic effects with an interface origin can be locally modified using a Ga^+ ion beam. In our analysis we have made several assumptions that are relevant for the interpretation of the obtained results. Here we explicitly list these assumption and discuss their consequences. (i) We assumed that the saturation magnetization is not affected by ion irradiation. This assumption is based on early work on the effect of Ga^+ ion irradiation of Pt|Co|Pt single magnetic layers. For comparable ion doses as those used in this article, either no or a small ($<5\%$) change in M_s is reported [36,46]. Both a decrease and increase could in theory occur, due to the intermixing of Co and Pt [36]. In Appendix B we show that a small decrease or increase in M_s does not influence the obtained results significantly. (ii) We assumed that the value of the exchange stiffness is equal to $A = 10$ pJ m and is not affected by the ion irradiation. The choice for the value of A is based on other work on similar magnetic multilayers [14,41,44]. In Appendix C we show that using a different value for A does not qualitatively affect the results. A change in the exchange stiffness due to ion irradiation has not been reported to the best of our knowledge and is not considered here. (iii) Finally, we did not directly consider the depth dependence of the ion irradiation. Contrary to lighter He^+ ions, Ga^+ ions have a significantly lower penetration depth resulting in a depth dependent damage profile [35,36]. The number of layers of the magnetic multilayer was chosen to ensure that all the layers are affected by the ion irradiation to some extent, as can be seen from the TRIM [56] simulations in Appendix D, while maximizing the number of layers to ensure, e.g., skyrmion stability. Although this depth dependence will mean that the magnetic parameters become depth dependent, the measurements reported in this article measure the effective anisotropy and effective iDMI, which correspond to the layer averaged values of these parameters. In the case

of the anisotropy measurement, this is straightforward to see, since the Hall signal is proportional to the average M_z inside the Hall cross. In Appendix E we show that this is also the case for the measurements of the iDMI.

To conclude, in this work we have investigated local tuning of the interface DMI and perpendicular magnetic anisotropy using Ga^+ ion irradiation, in an Ir|Co|Pt multilayer system. We showed that irradiation with Ga^+ ions has a significant effect on the interface contributions to both effects. The net effect of this is to reduce the energy cost of domain walls by up to a factor of 2, while still preserving their chiral Néel character. Hence, we postulate that Ga^+ ion irradiation is an effective way to locally—with a resolution of $\sim$40 nm— reduce the energy barrier for the nucleation of skyrmions and other chiral textures. Providing a novel pathway towards the control of chiral textures in future spintronic devices.

APPENDIX A: SQUID MEASUREMENTS ON UNPATTERNED [Ir(1)|Co(0.8)|Pt(1.0)]$_{\times 6}$

In this Appendix we present SQUID-VSM measurements of the saturation magnetization and effective anisotropy of the non-irradiated material stack [shown schematically in Fig. 4(a)]. In Fig. 4(b) we have plotted the normalized M-H curves for both an out-of-plane (OOP) and in-plane (IP) oriented magnetic field. M_s was measured to be $M_s = 1.01 \pm 0.04$ MA m^{-1}, to convert the measured moment $|\mathbf{m}|$ (in A m^2) to a magnetization we assumed that the total thickness of the magnetic volume is equal to the total Co thickness, 6×0.8 nm. The area between the IP and OOP loop (shaded with black lines) was used to calculate the effective anisotropy using the area method [43]. We find $K_{eff} = 0.47 \pm 0.05$ MJm^{-3}.
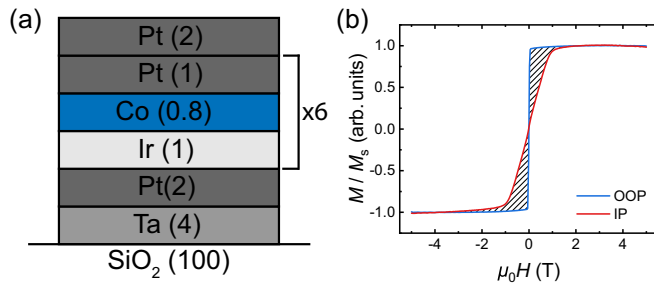
FIG. 4. (a) Schematic overview of the sample stack. (b) SQUID-VSM measurements of a 4×4 mm^2 sample of the non-irradiated multilayer shown in (a). The area between the in-plane (IP) and out-of-plane (OOP) loop (shaded with black lines) was used to calculate the effective anisotropy using the area method [43].

APPENDIX B: THE EFFECT OF SMALL CHANGES IN THE SATURATION MAGNETIZATION

In the main paper it was assumed that the saturation magnetization stays constant as a function of ion dose. This corresponds to measurements performed by Devolder [46]. However, Vieu *et al.* [36] estimate that small changes in M_s are possible for a system consisting of Pt|Co|Pt due to the formation of a Pt/Co alloy at larger doses. They find that M_s can change (increase or decrease) by approximately 5% for the maximum dose used in the main text. In Fig. 5 we show how our results would be affected by such a change. We assume here that M_s depends linearly on the dose.

The most significant effect is that the value found for the interface anisotropy will change, although the observed decrease upon irradiation is still clearly present as seen in Fig. 5(a). When M_s is increased, the Zeeman term in the Stoner-Wohlfarth model increases. Hence, to reproduce the experimentally observed behavior, the anisotropy term must also increase. Indeed, for an increasing M_s we find an increasing K_s and vice versa, compared to a constant M_s. In Fig. 5(b) we plot the interface DMI versus the interface anisotropy, for constant, increasing, and decreasing M_s. Here the behavior of M_s can slightly change the relative scaling of the two parameters as a function of dose, resulting in a faster or slower
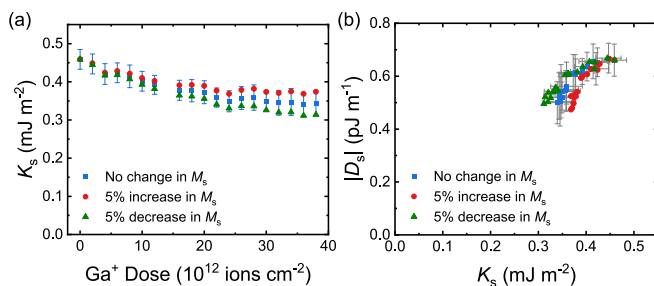

FIG. 5. (a) Plot of the interface anisotropy K_s as a function of ion dose. If M_s changes gradually as a function of dose, then the value of interface anisotropy determined using our measurement will change as well. (b) $|D_s|$ plotted as a function of K_s for constant (blue) and changing M_s (red and green). The error bars for the red and green data points are not shown in both figures, but are comparable in size to the blue data set.
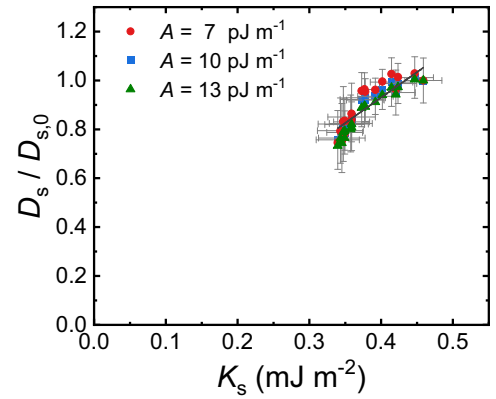

FIG. 6. Plot that shows how the results presented in Fig. 3(b) depend on the value of the exchange stiffness A. This plot is equivalent to Fig. 3(b) in the main text, with the only difference that we now plot the normalized interface DMI on the vertical axis. Each data set is normalized to the corresponding D_s for zero dose. The linear fit to the data and the error bars both correspond to the data set for $A = 10$ pJm^{-1}.

decrease in D_s compared to K_s. Nevertheless, this effect remains small and all values fall within the error bars shown in the main text.

APPENDIX C: THE VALUE OF THE EXCHANGE STIFFNESS

In this Appendix we examine the effect that the value of the exchange stiffness A has on the obtained results. To this end we have repeated the calculation of the interface DMI strength D_s for three different values of A. In Fig. 6 we plot these values for D_s as a function of the interface anisotropy K_s. Each dataset is normalized to the corresponding value of D_s for zero Ga$^+$ dose. When this is done for three different values of the exchange stiffness, we find that all the data overlap. In the main paper the value $A = 10$ pJm^{-1} was used. We conclude that the value of the iDMI D depends on A, but the effect of the ion irradiation reported in the main paper is independent of the value of A.

APPENDIX D: DEPTH DEPENDENCE OF THE Ga$^+$ ION IRRADIATION

The penetration depth of Ga$^+$ ions into Pt and Co is on the order of 10 nm [57]. Since the thickness of our magnetic multilayer system is larger, we expect that the effect of the ion irradiation is not uniform throughout the thickness of the multilayers. To get an estimate of the damage profile as a function of thickness, we have used the transport and ranges of ions in matter (TRIM) code [56] to simulate the effect of the impinging Ga$^+$ ions on the multilayers. The material stack that is implemented in the software is SiO$_2$|Ta(4)|Pt(2)|[R]$_{\times 6}$|Pt(2). Here R denotes the magnetic repeat Ir(1)|Co(0.8)|Pt(1). Due to limitations in the maximum layer number within the software, we were forced to model the repeat as an Ir : Co : Pt alloy, with a stoichiometric ratio of 10 : 8 : 10. In total 50 000 collision events are simulated, with 30 keV Ga$^+$ ions, corresponding to the irradiation applied in the experiment. In Fig. 7 we plot the average number of vacancies (dislocated
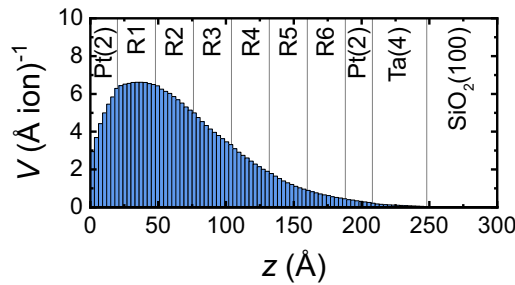
FIG. 7. Plot of the average number of vacancies created by each ion during the irradiation for a sample with six repeats, labeled R1 through R6. Each repeat consists of a 2.8 nm thick Ir : Co : Pt alloy with a stoichiometric ratio of 10 : 8 : 10. Simulations are performed using the TRIM code with a total of 50 000 ions with an energy of 30 keV.

atoms) created by each ion as a function of the depth into the magnetic multilayer. From this plot it is clear that there is a thickness dependence, with the top layers being influenced more strongly than the bottom layers. Based on these simulations the number of magnetic layers was limited to six in the main paper, to ensure that all layers are affected by the ion irradiation. Despite the thickness dependence, the results in the main paper show that the average magnetic interface properties of the stack are strongly influenced by the ion irradiation. In Appendix E we show using MuMax^3 that the measurement of the iDMI is still valid, even if there is a layer dependence in both the anisotropy and iDMI.

APPENDIX E: MuMax^3 SIMULATIONS OF NONUNIFORM IRRADIATION

Using MuMax^3 [53] we performed micromagnetic simulations of the magnetic multilayer stack after ion irradiation.

Here we investigate the correctness of the assumption that a measurement of the iDMI using the domain width in a stack in which the uniaxial anisotropy and iDMI vary as a function of layer number will result in the average iDMI parameter of the layers. The approach we take is similar to the approach used in Ref. [44], to verify their "averaging approach." The material system we simulate is [NM(2)/FM(1)] $\times N$, where $N = 6$ is the total number of repeats of the 2 nm thick nonmagnetic (NM) layer and 1 nm thick ferromagnetic (FM) layer. The average magnetic parameters are chosen to be equal to those of the stack irradiated with a Ga$^+$ dose of $d = 12 \times 10^{12}$ ions cm^2: $M_s = 1.0$ MA m^{-1}, $A = 10$ pJ m^{-1}, $K_u = 0.98$ MJ m^{-3}, and $D_{avg} = -1.5$ mJ m^{-2}. In the case of a nonuniform stack, both the uniaxial anisotropy and iDMI are layer dependent and vary linearly as a function of layer number (to approximate the depth dependence in Fig. 7). The difference between two successive layers is $\Delta K_u = 0.05$ MJ m^{-3} and $\Delta D = 0.05$ mJ m^{-2}, the average value of both parameters is equal to the corresponding value in the uniform stack. These differences between successive layers were chosen so that the value of D and K_u in the bottom layer are approximately the same as in the nonirradiated stack. Representing a scenario where the sixth layer is not affected by the irradiation, i.e., the largest possible gradient.

We simulate a region of 512 by 32 nm^2 with periodic boundary conditions in the x and y direction of 32 repeats. The cell sizes are given by $(x, y, z) = (0.5, 8, 1)$ nm. Two domain walls are then initialized in these systems, with the domain wall normal along the x direction. The width of these initial walls is set to 5 nm and the domain wall moment is set to 45° from the domain wall normal. The systems are subsequently relaxed, resulting in chiral Néel walls in all layers for both the uniform and nonuniform stack, as shown in Fig. 8(a). This is important because the model of Lemesh
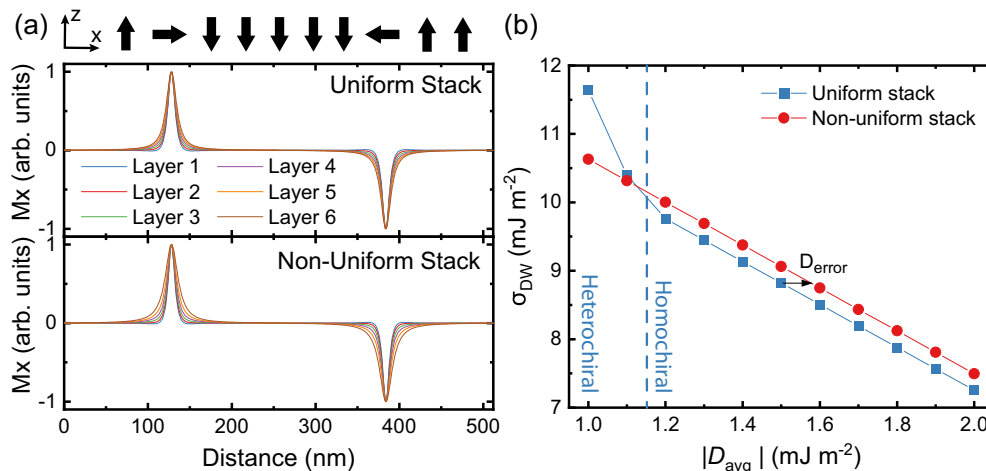

FIG. 8. (a) The x component of the magnetization in each of the six repeats, plotted for both the uniform and nonuniform stack. In both cases the domain walls have a clockwise chirality in all of the layers, for an average iDMI constant of $D_{avg} = -1.5$ mJ m^{-2} (illustrated by the arrows at the top of the figure). (b) Simulated domain wall energy density in the uniform and nonuniform systems. Above $|D_{avg}| = 1.2$ mJ m^{-2}, a linear dependence on D_{avg} is observed in both cases. Below this value the domain walls in the uniform stack no longer have the same chirality, resulting in a deviation from this linear dependence. In the nonuniform stack, the average domain wall energy density is slightly higher. The model of Lemesh [39] models a uniform stack, and therefore slightly underestimates the iDMI by $D_{error} \approx 0.08$ mJ m^{-2}, which falls well within the experimental uncertainty for D.

[39] assumes that the domain wall profile in each layer is the same. We also verified that for the largest ion dose used in this article, $d = 38 \times 10^{12}$ ions cm^{-2}, both scenarios results in CW Néel walls in all layers.

Next, we focus on extracting the domain wall energy density to verify that the model of Lemesh can still be used in the case of a gradient in K_u and D. We calculate the domain wall energy density by comparing the energy of the systems with domain walls to a uniformly magnetized system, the result is plotted in Fig. 8(b). Above $|D_{avg}| = 1.2$ mJ m^{-2}, a linear dependence of the domain wall energy on D_{avg} is observed in both cases. In the nonuniform stack, the domain wall energy density is slightly higher than in the uniform stack. The domain width in our measurements is determined by the domain wall energy and hence we look at the difference in D_{avg} that is present when the two systems have the same domain wall energy density. Since the model of Lemesh [39] assumes a uniform stack, this means that the iDMI is underestimated by $D_{error} \approx 0.08$ mJ m^{-2} in our measurements, which falls

entirely in our experimental uncertainty. Hence, the use of the model of Lemesh is a valid approach to calculate the average D in our system, even if a layer dependence of the magnetic parameters is present.

Below $|D_{avg}| = 1.2$ mJ m^{-2} the domain walls in the uniform stack no longer all have a CW chirality. The domain wall moments in the bottom of the stack rotate to align with the dipolar field, since the DMI is no longer strong enough to prevent this. This causes an increase in the domain wall energy density plotted in Fig. 8(b), because we do not include the dipolar energy. Interestingly, in the nonuniform scenario the domain walls in the simulation all kept their CW chirality. This can be understood because the DMI in the bottom layers is larger than in the top layers in this scenario and thus still strong enough to overcome the dipolar field. This suggests that a depth dependent irradiation profile (Ga$^+$ irradiation) might be beneficial over a uniform profile (He$^+$ irradiation) for multilayers, if the uniform chirality is important for the application.

---

[1] N. Nagaosa and Y. Tokura, Topological properties and dynamics of magnetic skyrmions, Nat. Nanotechnol. **8**, 899 (2013).

[2] R. Wiesendanger, Nanoscale magnetic skyrmions in metallic films and multilayers: A new twist for spintronics, Nat. Rev. Mater. **1**, 16044 (2016).

[3] A. Fert, N. Reyren, and V. Cros, Magnetic skyrmions: Advances in physics and potential applications, Nat. Rev. Mater. **2**, 17031 (2017).

[4] K. Everschor-Sitte, J. Masell, R. M. Reeve, and M. Kläui, Perspective: Magnetic skyrmions-Overview of recent progress in an active research field, J. Appl. Phys. **124**, 240901 (2018).

[5] A. N. Bogdanov and C. Panagopoulos, Physical foundations and basic properties of magnetic skyrmions, Nat. Rev. Phys. **2**, 492 (2020).

[6] F. Büttner, I. Lemesh, and G. S. D. Beach, Theory of isolated magnetic skyrmions: From fundamentals to room temperature applications, Sci. Rep. **8**, 4464 (2018).

[7] S. Woo, K. Litzius, B. Krüger, M.-Y. Im, L. Caretta, K. Richter, M. Mann, A. Krone, R. M. Reeve, M. Weigand, P. Agrawal, I. Lemesh, M.-A. Mawass, P. Fischer, M. Kläui, and G. S. D. Beach, Observation of room-temperature magnetic skyrmions and their current-driven dynamics in ultrathin metallic ferromagnets, Nat. Mater. **15**, 501 (2016).

[8] S. Rohart, J. Miltat, and A. Thiaville, Path to collapse for an isolated Néel skyrmion, Phys. Rev. B **93**, 214412 (2016).

[9] S.-G. Je, H.-S. Han, S. K. Kim, S. A. Montoya, W. Chao, I.-S. Hong, E. E. Fullerton, K.-S. Lee, K.-J. Lee, M.-Y. Im, and J.-I. Hong, Direct demonstration of topological stability of magnetic skyrmions via topology manipulation, ACS Nano **14**, 3251 (2020).

[10] I. Dzyaloshinsky, A thermodynamic theory of "weak" ferromagnetism of antiferromagnetics, J. Phys. Chem. Solids **4**, 241 (1958).

[11] T. Moriya, Anisotropic superexchange interaction and weak ferromagnetism, Phys. Rev. **120**, 91 (1960).

[12] N. Kanazawa, S. Seki, and Y. Tokura, Noncentrosymmetric magnets hosting magnetic skyrmions, Adv. Mater. **29**, 1603227 (2017).

[13] N. Mathur, M. J. Stolt, and S. Jin, Magnetic skyrmions in nanostructures of non-centrosymmetric materials, APL Mater. **7**, 120703 (2019).

[14] C. Moreau-Luchaire, C. Moutafis, N. Reyren, J. Sampaio, C. A. F. Vaz, N. Van Horne, K. Bouzehouane, K. Garcia, C. Deranlot, P. Warnicke, P. Wohlhüter, J.-M. George, M. Weigand, J. Raabe, V. Cros, and A. Fert, Additive interfacial chiral interaction in multilayers for stabilization of small individual skyrmions at room temperature, Nat. Nanotechnol. **11**, 444 (2016).

[15] O. Boulle, J. Vogel, H. Yang, S. Pizzini, D. de Souza Chaves, A. Locatelli, T. O. Menteş, A. Sala, L. D. Buda-Prejbeanu, O. Klein, M. Belmeguenai, Y. Roussigné, A. Stashkevich, S. M. Chérif, L. Aballe, M. Foerster, M. Chshiev, S. Auffret, I. M. Miron, and G. Gaudin, Room-temperature chiral magnetic skyrmions in ultrathin magnetic nanostructures, Nat. Nanotechnol. **11**, 449 (2016).

[16] A. Soumyanarayanan, M. Raju, A. L. Gonzalez Oyarce, A. K. C. Tan, M.-Y. Im, A. P. Petrović, P. Ho, K. H. Khoo, M. Tran, C. K. Gan, F. Ernult, and C. Panagopoulos, Tunable room-temperature magnetic skyrmions in Ir/Fe/Co/Pt multilayers, Nat. Mater. **16**, 898 (2017).

[17] F. Büttner, I. Lemesh, M. Schneider, B. Pfau, C. M. Günther, P. Hessing, J. Geilhufe, L. Caretta, D. Engel, B. Krüger, J. Viefhaus, S. Eisebitt, and G. S. D. Beach, Field-free deterministic ultrafast creation of magnetic skyrmions by spin-orbit torques, Nat. Nanotechnol. **12**, 1040 (2017).

[18] M. He, L. Peng, Z. Zhu, G. Li, J. Cai, J. Li, H. Wei, L. Gu, S. Wang, T. Zhao, B. Shen, and Y. Zhang, Realization of zero-field skyrmions with high-density via electromagnetic manipulation in Pt/Co/Ta multilayers, Appl. Phys. Lett. **111**, 202403 (2017).

[19] W. Legrand, D. Maccariello, N. Reyren, K. Garcia, C. Moutafis, C. Moreau-Luchaire, S. Collin, K. Bouzehouane, V. Cros, and

A. Fert, Room-temperature current-induced generation and motion of sub-100 nm skyrmions, Nano Lett. **17**, 2703 (2017).

[20] I. Lemesh, K. Litzius, M. Böttcher, P. Bassirian, N. Kerber, D. Heinze, J. Zázvorka, F. Büttner, L. Caretta, M. Mann, M. Weigand, S. Finizio, J. Raabe, M.-Y. Im, H. Stoll, G. Schütz, B. Dupé, M. Kläui, and G. S. D. Beach, Current-induced skyrmion generation through morphological thermal transitions in chiral ferromagnetic heterostructures, Adv. Mater. **30**, 1805461 (2018).

[21] S. Zhang, J. Zhang, Y. Wen, E. M. Chudnovsky, and X. Zhang, Creation of a thermally assisted skyrmion lattice in Pt/Co/Ta multilayer films, Appl. Phys. Lett. **113**, 192403 (2018).

[22] S. Finizio, K. Zeissler, S. Wintz, S. Mayr, T. Weßels, A. J. Huxtable, G. Burnell, C. H. Marrows, and J. Raabe, Deterministic field-free skyrmion nucleation at a nanoengineered injector device, Nano Lett. **19**, 7246 (2019).

[23] J. A. Brock, S. A. Montoya, M.-Y. Im, and E. E. Fullerton, Energy-efficient generation of skyrmion phases in Co/Ni/Pt-based multilayers using Joule heating, Phys. Rev. Mater. **4**, 104409 (2020).

[24] F. Büttner, B. Pfau, M. Böttcher, M. Schneider, G. Mercurio, C. M. Günther, P. Hessing, C. Klose, A. Wittmann, K. Gerlinger, L.-M. Kern, C. Strüber, C. von Korff Schmising, J. Fuchs, D. Engel, A. Churikova, S. Huang, D. Suzuki, I. Lemesh, M. Huang *et al.*, Observation of fluctuation-mediated picosecond nucleation of a topological phase, Nat. Mater. **20**, 30 (2021).

[25] I. Purnama, W. L. Gan, D. W. Wong, and W. S. Lew, Guided current-induced skyrmion motion in 1D potential well, Sci. Rep. **5**, 10620 (2015).

[26] P. Lai, G. P. Zhao, H. Tang, N. Ran, S. Q. Wu, J. Xia, X. Zhang, and Y. Zhou, An improved racetrack structure for transporting a skyrmion, Sci. Rep. **7**, 45330 (2017).

[27] R. Juge, K. Bairagi, K. G. Rana, J. Vogel, M. Sall, D. Mailly, V. T. Pham, Q. Zhang, N. Sisodia, M. Foerster, L. Aballe, M. Belmeguenai, Y. Roussigné, S. Auffret, L. D. Buda-Prejbeanu, G. Gaudin, D. Ravelosona, and O. Boulle, Helium ions put magnetic skyrmions on the track, Nano Lett. **21**, 2989 (2021).

[28] K. Ohara, X. Zhang, Y. Chen, Z. Wei, Y. Ma, J. Xia, Y. Zhou, and X. Liu, Confinement and protection of skyrmions by patterns of modified magnetic properties, Nano Lett. **21**, 4320 (2021).

[29] K. Everschor-Sitte, M. Sitte, T. Valet, A. Abanov, and J. Sinova, Skyrmion production on demand by homogeneous DC currents, New J. Phys. **19**, 092001 (2017).

[30] K. Fallon, S. Hughes, K. Zeissler, W. Legrand, F. Ajejas, D. Maccariello, S. McFadzean, W. Smith, D. McGrouther, S. Collin, N. Reyren, V. Cros, C. H. Marrows, and S. McVitie, Controlled individual skyrmion nucleation at artificial defects formed by ion irradiation, Small **16**, 1907450 (2020).

[31] J. H. Franken, M. Hoeijmakers, R. Lavrijsen, J. T. Kohlhepp, H. J. M. Swagten, B. Koopmans, E. van Veldhoven, and D. J. Maas, Precise control of domain wall injection and pinning using helium and gallium focused ion beams, J. Appl. Phys. **109**, 07D504 (2011).

[32] A. L. Balk, K.-W. Kim, D. T. Pierce, M. D. Stiles, J. Unguris, and S. M. Stavis, Simultaneous Control of the Dzyaloshinskii-Moriya Interaction and Magnetic Anisotropy in Nanomagnetic Trilayers, Phys. Rev. Lett. **119**, 077205 (2017).

[33] X. Zhao, B. Zhang, N. Vernier, X. Zhang, M. Sall, T. Xing, L. Herrera Diez, C. Hepburn, L. Wang, G. Durin, A. Casiraghi, M. Belmeguenai, Y. Roussigné, A. Stashkevich, S. M. Chérif, J. Langer, B. Ocker, S. Jaiswal, G. Jakob, M. Kläui *et al.*, Enhancing domain wall velocity through interface intermixing in W-CoFeB-MgO films with perpendicular anisotropy, Appl. Phys. Lett. **115**, 122404 (2019).

[34] L. H. Diez, M. Voto, A. Casiraghi, M. Belmeguenai, Y. Roussigné, G. Durin, A. Lamperti, R. Mantovan, V. Sluka, V. Jeudy, Y. T. Liu, A. Stashkevich, S. M. Chérif, J. Langer, B. Ocker, L. Lopez-Diaz, and D. Ravelosona, Enhancement of the Dzyaloshinskii-Moriya interaction and domain wall velocity through interface intermixing in Ta/CoFeB/MgO, Phys. Rev. B **99**, 054431 (2019).

[35] A. Sud, S. Tacchi, D. Sagkovits, C. Barton, M. Sall, L. H. Diez, E. Stylianidis, N. Smith, L. Wright, S. Zhang, X. Zhang, D. Ravelosona, G. Carlotti, H. Kurebayashi, O. Kazakova, and M. Cubukcu, Tailoring interfacial effect in multilayers with Dzyaloshinskii-Moriya interaction by helium ion irradiation, Sci. Rep. **11**, 23626 (2021).

[36] C. Vieu, J. Gierak, H. Launois, T. Aign, P. Meyer, J. P. Jamet, J. Ferré, C. Chappert, T. Devolder, V. Mathet, and H. Bernas, Modifications of magnetic properties of Pt/Co/Pt thin layers by focused gallium ion beam irradiation, J. Appl. Phys. **91**, 3103 (2002).

[37] R. Lavrijsen, Another spin in the wall : Domain wall dynamics in perpendicularly magnetized devices, Ph.D. thesis, University of Technology Eindhoven, 2011.

[38] J. Franken, Domain walls shift gears—Novel ways to control magnetic domain-wall motion, Ph.D. thesis, University of Technology Eindhoven, 2014.

[39] I. Lemesh, F. Büttner, and G. S. D. Beach, Accurate model of the stripe domain phase of perpendicularly magnetized multilayers, Phys. Rev. B **95**, 174423 (2017).

[40] P. Agrawal, F. Büttner, I. Lemesh, S. Schlotter, and G. S. D. Beach, Measurement of interfacial Dzyaloshinskii-Moriya interaction from static domain imaging, Phys. Rev. B **100**, 104430 (2019).

[41] W. Legrand, J.-Y. Chauleau, D. Maccariello, N. Reyren, S. Collin, K. Bouzehouane, N. Jaouen, V. Cros, and A. Fert, Hybrid chiral domain walls and skyrmions in magnetic multilayers, Sci. Adv. **4**, eaat0415 (2018).

[42] S. Schlotter, P. Agrawal, and G. S. D. Beach, Temperature dependence of the Dzyaloshinskii-Moriya interaction in Pt/Co/Cu thin film heterostructures, Appl. Phys. Lett. **113**, 092402 (2018).

[43] M. T. Johnson, P. J. H. Bloemen, F. J. A. den Broeder, and J. J. de Vries, Magnetic anisotropy in metallic multilayers, Rep. Prog. Phys. **59**, 1409 (1996).

[44] J. Lucassen, M. J. Meijer, M. C. H. de Jong, R. A. Duine, H. J. M. Swagten, B. Koopmans, and R. Lavrijsen, Stabilizing chiral spin structures via an alternating Dzyaloshinskii-Moriya interaction, Phys. Rev. B **102**, 014451 (2020).

[45] N. Nagaosa, J. Sinova, S. Onoda, A. H. MacDonald, and N. P. Ong, Anomalous Hall effect, Rev. Mod. Phys. **82**, 1539 (2010).

[46] T. Devolder, Light ion irradiation of Co/Pt systems: Structural origin of the decrease in magnetic anisotropy, Phys. Rev. B **62**, 5794 (2000).

[47] H. Yang, A. Thiaville, S. Rohart, A. Fert, and M. Chshiev, Anatomy of Dzyaloshinskii-Moriya Interaction at Co/Pt Interfaces, Phys. Rev. Lett. **115**, 267210 (2015).

[48] B. Zimmermann, W. Legrand, D. Maccariello, N. Reyren, V. Cros, S. Blügel, and A. Fert, Dzyaloshinskii-Moriya interaction at disordered interfaces from *ab initio* theory: Robustness against intermixing and tunability through dusting, Appl. Phys. Lett. **113**, 232403 (2018).

[49] J. Lucassen, F. Kloodt-Twesten, R. Frömter, H. P. Oepen, R. A. Duine, H. J. M. Swagten, B. Koopmans, and R. Lavrijsen, Scanning electron microscopy with polarization analysis for multilayered chiral spin textures, Appl. Phys. Lett. **111**, 132403 (2017).

[50] A. Thiaville, S. Rohart, E. Jue, V. Cros, and A. Fert, Dynamics of Dzyaloshinskii domain walls in ultrathin magnetic films, Europhys. Lett. **100**, 57002 (2012).

[51] Y. Dovzhenko, F. Casola, S. Schlotter, T. X. Zhou, F. Büttner, R. L. Walsworth, G. S. D. Beach, and A. Yacoby, Magnetostatic twists in room-temperature skyrmions explored by nitrogen-vacancy center spin texture reconstruction, Nat. Commun. **9**, 2712 (2018).

[52] I. Lemesh and G. S. D. Beach, Twisted domain walls and skyrmions in perpendicularly magnetized multilayers, Phys. Rev. B **98**, 104402 (2018).

[53] A. Vansteenkiste, J. Leliaert, M. Dvornik, M. Helsen, F. Garcia-Sanchez, and B. Van Waeyenberge, The design and verification of MuMax3, AIP Adv. **4**, 107133 (2014).

[54] W.-Y. Kim, H. K. Gweon, K.-J. Lee, and C.-Y. You, Correlation between interfacial Dzyaloshinskii-Moriya interaction and interfacial magnetic anisotropy of Pt/Co/MgO structures, Appl. Phys. Express **12**, 053007 (2019).

[55] G. W. Kim, A. S. Samardak, Y. J. Kim, I. H. Cha, A. V. Ognev, A. V. Sadovnikov, S. A. Nikitov, and Y. K. Kim, Role of the Heavy Metal's Crystal Phase in Oscillations of Perpendicular Magnetic Anisotropy and the Interfacial Dzyaloshinskii-Moriya Interaction in W/Co-Fe-B/MgO Films, Phys. Rev. Appl. **9**, 064005 (2018).

[56] J. F. Ziegler, M. Ziegler, and J. Biersack, SRIM - The stopping and range of ions in matter (2010), Nucl. Instrum. Methods Phys. Res. Sect. B **268**, 1818 (2010).

[57] R. Hyndman, P. Warin, J. Gierak, J. Ferré, J. N. Chapman, J. P. Jamet, V. Mathet, and C. Chappert, Modification of Co/Pt multilayers by gallium irradiation-Part 1: The effect on structural and magnetic properties, J. Appl. Phys. **90**, 3843 (2001).